ALTERNATIVE FORM OF BOUSSINESQ EQUATIONS FOR NEARSHORE WAVE PROPAGATION

By Okey Nwogu[1]

ABSTRACT: Boussinesq-type equations can be used to model the nonlinear transformation of surface waves in shallow water due to the effects of shoaling, refraction, diffraction, and reflection. Different linear dispersion relations can be obtained by expressing the equations in different velocity variables. In this paper, a new form of the Boussinesq equations is derived using the velocity at an arbitrary distance from the still water level as the velocity variable instead of the commonly used depth-averaged velocity. This significantly improves the linear dispersion properties of the Boussinesq equations, making them applicable to a wider range of water depths. A finite difference method is used to solve the equations. Numerical and experimental results are compared for the propagation of regular and irregular waves on a constant slope beach. The results demonstrate that the new form of the equations can reasonably simulate several nonlinear effects that occur in the shoaling of surface waves from deep to shallow water including the amplification of the forced lower- and higher-frequency wave harmonics and the associated increase in the horizontal and vertical asymmetry of the waves.

INTRODUCTION

As surface waves propagate from deep to shallow water, the wave field is transformed due to the effects of shoaling, refraction, diffraction and reflection. Boussinesq-type equations for water of varying depth, derived by Peregrine (1967), are able to describe the nonlinear transformation of irregular, multidirectional waves in shallow water. Boussinesq equations represent the depth-integrated equations for the conservation of mass and momentum for an incompressible and inviscid fluid. The vertical velocity is assumed to vary linearly over the depth to reduce the three-dimensional problem to a two-dimensional one.

The Boussinesq equations include the lowest-order effects of frequency dispersion and nonlinearity. They can thus account for the transfer of energy between different frequency components, changes in the shape of the individual waves, and the evolution of the wave groups, in the shoaling of an irregular wave train (e.g., Freilich and Guza 1984). A major limitation of the commonly used form of the Boussinesq equations is that they are only applicable to relatively shallow water depths. To keep errors in the phase velocity less than 5%, the water depth has to be less than about one-fifth of the equivalent deep-water wavelength (McCowan 1987).

Recently, a number of attempts have been made to extend the range of applicability of the equations to deeper water by improving the dispersion characteristics of the equations. Witting (1984) used a different form of the exact, fully nonlinear, depth-integrated momentum equation for one horizontal dimension, expressed in terms of the velocity at the free surface. A Taylor-series–type expansion was used to relate the different velocity var-

[1]Res. Officer, Hydr. Lab., Inst. for Mech. Engrg., Nat. Res. Council, Ottawa, Ontario K1A 0R6, Canada.

Note. Discussion open until May 1, 1994. To extend the closing date one month, a written request must be filed with the ASCE Manager of Journals. The manuscript for this paper was submitted for review and possible publication on August 31, 1992. This paper is part of the ***Journal of Waterway, Port, Coastal, and Ocean Engineering***, Vol. 119, No. 6, November/December, 1993. ©ASCE, ISSN 0733-950X/93/0006-0618/$1.00 + $.15 per page. Paper No. 4696.

iables in the governing equations, with the coefficients of the expansion determined to yield the best linear dispersion characteristics. By retaining terms up to the fourth order in dispersion, Witting obtained relatively accurate results for both deep and shallow water waves. However, an exact form of depth integrated momentum equation cannot be easily derived for two horizontal dimensions, and the expansions presented by Witting are only valid in water of constant depth.

Murray (1989) and Madsen et al. (1991) examined the dispersion properties of various forms of the Boussinesq equations as well as Witting's (1984) Padé approximation of the linear dispersion relation for Airy waves. Based on the excellent characteristics of the Padé approximant, the writers have introduced an additional third-order term to the momentum equation to improve the dispersion properties of the Boussinesq equations. The third-order term is derived from the long wave equations and reduces to zero in shallow water, resulting in the standard form of the equations for shallow water. The equations assume a constant water depth and, thus, are not applicable to shoaling waves.

A different approach was used by McCowan and Blackman (1989), who used an effective depth concept to restrict the depth integration to the upper part of the water column in deeper water. For any given wave frequency, the effective depth is chosen to match the dispersion properties of Airy waves. Such an approach, however, is only applicable to regular waves.

In this paper, an alternative form of the two-dimensional Boussinesq equations for water of variable depth is derived, using the velocity at an arbitrary distance from the still water level as the velocity variable. The resulting linear dispersion relation of the new set of equations is similar to that presented by Witting (1984), and later used by Murray (1989) and Madsen et al. (1991). However, the equations presented in this paper are consistently derived from the continuity and Euler's equations of motion, and are applicable to waves propagating in water of variable depth. A finite difference method is used to solve the equations for one horizontal dimension. The results of the numerical model are compared with laboratory data for the shoaling of regular and irregular waves on a constant slope beach.

NEW SET OF BOUSSINESQ-TYPE EQUATIONS

Derivation of Equations

There are different methods of deriving the Boussinesq equations. One approach is the perturbation method, used by Peregrine (1967). A different approach was used by Yoon and Liu (1989) to derive a set of equations that included the effect of wave-current interaction. In this section, a method similar to that employed by Yoon and Liu is used to derive a new class of Boussinesq-type equations. The velocity at an arbitrary elevation is used as the velocity variable, instead of the commonly used depth-averaged velocity.

Consider a three-dimensional wave field with water-surface elevation $\eta\ (x, y, t)$, at time t, propagating over a variable water depth $h(x, y)$. A Cartesian coordinate system (x, y, z) is adopted, with z measured upwards from the still-water level. The fluid is assumed to be inviscid and incompressible, and the flow is assumed to be irrotational. Two important length scales are the characteristic water depth h_0 for the vertical direction and a typical wavelength l for the horizontal direction. The variables associated with the different length scales are considered to be of different orders of magnitude. The following independent, nondimensional variables can be defined:

$$x = \frac{x'}{l}, \quad y = \frac{y'}{l}, \quad z = \frac{z'}{h_0}, \quad t = \frac{\sqrt{gh_0}}{l} t' \quad \ldots\ldots (1)$$

where g = gravitational acceleration; and primes are used to denote dimensional variables. For effects due to the motion of the free surface, the typical wave amplitude a_0 is also important. The following dependent, nondimensional variables can also be defined:

$$u = \frac{h_0}{a_0\sqrt{gh_0}} u', \quad v = \frac{h_0}{a_0\sqrt{gh_0}} v', \quad w = \frac{h_0^2}{a_0 l\sqrt{gh_0}} w' \quad \ldots\ldots (2a)$$

$$\eta = \frac{\eta'}{a_0}, \quad h = \frac{h'}{h_0}, \quad p = \frac{p'}{\rho g a_0} \quad \ldots\ldots (2b)$$

where (u, v, w) = the water particle velocity vector; p = the pressure; and ρ = the fluid density. The governing equations for the fluid motion are the continuity equation and Euler's equations of motion. The continuity equation can be expressed in nondimensional form as:

$$\mu^2(u_x + v_y) + w_z = 0 \quad \ldots\ldots (3)$$

Euler's equations of motion can be expressed in nondimensional form as:

$$\mu^2 u_t + \varepsilon\mu^2 u u_x + \varepsilon\mu^2 v u_y + \varepsilon w u_z + \mu^2 p_x = 0 \quad \ldots\ldots (4)$$

$$\mu^2 v_t + \varepsilon\mu^2 u v_x + \varepsilon\mu^2 v v_y + \varepsilon w v_z + \mu^2 p_y = 0 \quad \ldots\ldots (5)$$

$$\varepsilon w_t + \varepsilon^2 u w_x + \varepsilon^2 v w_y + \frac{\varepsilon^2}{\mu^2} w w_z + \varepsilon p_z + 1 = 0 \quad \ldots\ldots (6)$$

The parameters $\varepsilon = a_0/h_0$ and $\mu = h_0/l$ are measures of nonlinearity and frequency dispersion, respectively, and are assumed to be small. The irrotationality condition is given by

$$u_y - v_x = 0, \quad v_z - w_y = 0, \quad w_x - u_z = 0 \quad \ldots\ldots (7)$$

The fluid has to satisfy a dynamic boundary condition at the free surface and kinematic boundary conditions at the free surface and seabed. These can be expressed as:

$$p = 0, \quad \text{at } z = \varepsilon\eta \quad \ldots\ldots (8)$$

$$w = \mu^2\eta_t + \varepsilon\mu^2 u\eta_x + \varepsilon\mu^2 v\eta_y, \quad \text{at } z = \varepsilon\eta \quad \ldots\ldots (9)$$

$$w = -\mu^2 u h_x - \mu^2 v h_y, \quad \text{at } z = -h \quad \ldots\ldots (10)$$

For the horizontal propagation of waves, the three-dimensional problem can be reduced to a two-dimensional one by integrating the equations over the water depth. Integrating the continuity equation [(3)] from the seabed to the free surface and applying the kinematic boundary conditions in (9) and (10) results in:

$$\frac{\partial}{\partial x}\int_{-h}^{\varepsilon\eta} u\, dz + \frac{\partial}{\partial y}\int_{-h}^{\varepsilon\eta} v\, dz + \eta_t = 0 \quad \ldots\ldots (11)$$

Similarly, the horizontal momentum equations [(4) and (5)] can be integrated over the depth to give:

$$\frac{\partial}{\partial t}\int_{-h}^{\varepsilon\eta} u\,dz + \varepsilon\frac{\partial}{\partial x}\int_{-h}^{\varepsilon\eta} u^2\,dz + \varepsilon\frac{\partial}{\partial y}\int_{-h}^{\varepsilon\eta} uv\,dz + \frac{\partial}{\partial x}\int_{-h}^{\varepsilon\eta} p\,dz$$

$$- p|_{z=-h}h_x = 0 \quad \ldots\ldots (12)$$

$$\frac{\partial}{\partial t}\int_{-h}^{\varepsilon\eta} v\,dz + \varepsilon\frac{\partial}{\partial x}\int_{-h}^{\varepsilon\eta} uv\,dz + \varepsilon\frac{\partial}{\partial y}\int_{-h}^{\varepsilon\eta} v^2\,dz + \frac{\partial}{\partial y}\int_{-h}^{\varepsilon\eta} p\,dz$$

$$- p|_{z=-h}h_y = 0 \quad \ldots\ldots (13)$$

where (3) and (8)–(10) have been used. Details of the integration procedure can be found in Phillips (1977) and Mei (1983). The pressure field is obtained by integrating the vertical momentum equation [(6)] with respect to z and applying the boundary conditions in (8) and (9) at the free surface:

$$p = \eta - \frac{z}{\varepsilon} + \frac{\partial}{\partial t}\int_{z}^{\varepsilon\eta} w\,dz + \varepsilon\frac{\partial}{\partial x}\int_{z}^{\varepsilon\eta} uw\,dz + \varepsilon\frac{\partial}{\partial y}\int_{z}^{\varepsilon\eta} vw\,dz - \frac{\varepsilon}{\mu^2}w^2 \quad \ldots\ldots (14)$$

Finally, the vertical velocity w is obtained by integrating the continuity equation [(3)] with respect to z and applying the seabed condition [(10)]:

$$w = -\mu^2\left(\frac{\partial}{\partial x}\int_{-h}^{z} u\,dz + \frac{\partial}{\partial y}\int_{-h}^{z} v\,dz\right) \quad \ldots\ldots (15)$$

All the foregoing equations are exact, and are valid for all orders of ε and μ. To integrate these equations, the depth dependence of the variables must be known. One approach might be to assume the hyperbolic cosine variation of Airy waves over depth. However, the resulting equations would only be applicable to regular waves since the hyperbolic function depends on the wave frequency.

A different approach, consistent with Boussinesq theory, is a perturbation from long wave theory to include the effect of frequency dispersion. The horizontal velocities are initially expanded as a Taylor series about the seabed ($z = -h$):

$$\mathbf{u}(x, y, z, t) = \mathbf{u}(x, y, -h, t) + (z + h)\mathbf{u}_z(x, y, -h, t)$$

$$+ \frac{(z + h)^2}{2}\mathbf{u}_{zz}(x, y, -h, t) + \cdots \quad \ldots\ldots (16)$$

where $\mathbf{u} = (u, v)$. Subsituting (15) for the vertical velocity into the irrotationality condition [(7)] and evaluating at the seabed yields:

$$\mathbf{u}_z(x, y, -h, t) = -\mu^2[\nabla(\mathbf{u}_b\cdot\nabla h) + (\nabla\cdot\mathbf{u})|_{z=-h}\nabla h] \quad \ldots\ldots (17)$$

where $\mathbf{u}_b = \mathbf{u}(x, y, -h, t)$ = the velocity at the bottom; and $\nabla = (\partial/\partial x, \partial/\partial y)$. Substituting (16) and (17) into (15) and integrating gives:

$$w = -\mu^2\nabla\cdot[(z + h)\mathbf{u}_b] + \mu^4\nabla\cdot\left[\frac{(z + h)^2}{2}[\nabla(\mathbf{u}_b\cdot\nabla h)\right.$$

$$\left. + (\nabla\cdot\mathbf{u})|_{z=-h}\nabla h]\right] + O(\mu^6) \quad \ldots\ldots (18)$$

Assuming that ∇h is of $O(1)$, w varies linearly over the depth to the leading order in frequency dispersion, $O(\mu^2)$. The horizontal velocities can be ex-

pressed in terms of the bottom velocity by integrating the irrotationality condition [(7)] over depth, that is

$$\mathbf{u} - \mathbf{u}_b = \int_{-h}^{z} \nabla w \, dz \quad \text{(19)}$$

Substituting (18) for w into (19) and integrating gives

$$\mathbf{u} = \mathbf{u}_b + \mu^2 \left(\frac{h^2}{2} - \frac{z^2}{2} \right) \nabla(\nabla \cdot \mathbf{u}_b) - \mu^2 (h + z) \nabla[\nabla \cdot (h\mathbf{u}_b)] + O(\mu^4) \quad \text{(20)}$$

To $O(\mu^2)$, the horizontal velocities vary quadratically over the depth. If we assume that $O(\varepsilon) = O(\mu^2) << 1$, the pressure field can be obtained by substituting (20) for $\mathbf{u}$ and (18) for w into (14) and integrating, retaining terms up to $O(\varepsilon)$ and $O(\mu^2)$:

$$p = \eta - \frac{z}{\varepsilon} + \mu^2 z \nabla \cdot (h\mathbf{u}_{bt}) + \mu^2 \frac{z^2}{2} \nabla \cdot \mathbf{u}_{bt} + O(\varepsilon^2, \varepsilon\mu^2, \mu^4) \quad \text{(21)}$$

The vertical distribution of the pressure is also quadratic. Instead of using the bottom velocity or the depth-averaged velocity as the velocity variable, the velocity $\mathbf{u}_\alpha$ at an arbitrary elevation $z = z_\alpha(x, y)$ may be used. The velocities and pressure can be expressed in terms of $\mathbf{u}_\alpha$ as:

$$w = -\mu^2 \nabla \cdot (h\mathbf{u}_\alpha) - \mu^2 z \nabla \cdot \mathbf{u}_\alpha + O(\mu^4) \quad \text{(22)}$$

$$\mathbf{u} = \mathbf{u}_\alpha + \mu^2 \left(\frac{z_\alpha^2}{2} - \frac{z^2}{2} \right) \nabla(\nabla \cdot \mathbf{u}_\alpha) + \mu^2 (z_\alpha - z) \nabla[\nabla \cdot (h\mathbf{u}_\alpha)] + O(\mu^4) \quad \text{(23)}$$

and

$$p = \eta - \frac{z}{\varepsilon} + \mu^2 z \nabla \cdot (h\mathbf{u}_{\alpha t}) + \mu^2 \frac{z^2}{2} \nabla \cdot \mathbf{u}_{\alpha t} + O(\varepsilon^2, \varepsilon\mu^2, \mu^4) \quad \text{(24)}$$

Substituting (22)–(24) into the depth-integrated continuity and horizontal momentum equations [(11)–(13)] and integrating, retaining terms up to $O(\varepsilon)$ and $O(\mu^2)$, we obtain a new set of Boussinesq-type equations:

$$\eta_t + \nabla \cdot [(h + \varepsilon\eta)\mathbf{u}_\alpha] + \mu^2 \nabla \cdot \left\{ \left(\frac{z_\alpha^2}{2} - \frac{h^2}{6} \right) h \nabla(\nabla \cdot \mathbf{u}_\alpha) + \left(z_\alpha + \frac{h}{2} \right) h \nabla[\nabla \cdot (h\mathbf{u}_\alpha)] \right\} = 0 \quad \text{(25a)}$$

$$\mathbf{u}_{\alpha t} + \nabla\eta + \varepsilon(\mathbf{u}_\alpha \cdot \nabla)\mathbf{u}_\alpha + \mu^2 \left\{ \frac{z_\alpha^2}{2} \nabla(\nabla \cdot \mathbf{u}_{\alpha t}) + z_\alpha \nabla[\nabla \cdot (h\mathbf{u}_{\alpha t})] \right\} = 0 \quad \text{(25b)}$$

This new set of equations can model the horizontal propagation of irregular, multi-directional waves in water of varying depth, provided $O(\varepsilon) = O(\mu^2) << 1$, and $O(\nabla h) = O(1)$. The standard form of the Boussinesq equations (Peregrine 1967) which uses the depth-averaged velocity, $\bar{\mathbf{u}}$, as the velocity variable can be written as:

$$\eta_t + \nabla \cdot [(h + \varepsilon\eta)\bar{\mathbf{u}}] = 0 \quad \text{(26a)}$$

$$\bar{\mathbf{u}}_t + \nabla\eta + \varepsilon(\bar{\mathbf{u}}\cdot\nabla)\bar{\mathbf{u}} + \mu^2\left\{\frac{h^2}{6}\nabla(\nabla\cdot\bar{\mathbf{u}}_t) - \frac{h}{2}\nabla[\nabla\cdot(h\bar{\mathbf{u}}_t)]\right\} = 0 \quad \ldots\ldots (26b)$$

Compared to the commonly used form of the Boussinesq equations, the new equations contain an additional frequency dispersion term in the continuity equation. It is shown in the next section that the linear dispersion characteristics of the new set of equations may be quite different from that of the standard set of equations, especially in intermediate and deep water.

Linear Dispersion Properties

The new set of equations [(25*a*) and (25*b*)] may be regarded as a class of equations containing most known forms of Boussinesq-type equations, with the elevation of the velocity variable, z_α, as a free parameter. The different possible velocity variables include the velocity at the seabed and the velocity at the still-water level. Since the equations are an approximation of the fully dispersive and nonlinear problem, one can select a velocity variable to minimize the errors introduced by the approximation. In this paper, we consider the linear limit and choose z_α to obtain the best fit between the linear dispersion relation of the model and the exact dispersion relation for a wide range of water depths. The linearized version of the equations for one horizontal dimension and constant depth can be expressed in dimensional form as:

$$\eta_t + hu_{\alpha x} + \left(\alpha + \frac{1}{3}\right)h^3u_{\alpha xxx} = 0 \quad \ldots\ldots (27)$$

$$u_{\alpha t} + g\eta_x + \alpha h^2u_{\alpha xxt} = 0 \quad \ldots\ldots (28)$$

where $\alpha = (z_\alpha/h)^2/2 + (z_\alpha/h)$; and the primes have been dropped. Consider a small amplitude periodic wave with frequency ω and wave number k:

$$\eta = a_0\exp[i(kx - \omega t)], \quad u_\alpha = u_0\exp[i(kx - \omega t)] \quad \ldots\ldots (29)$$

Substituting (29) into (27) and (28) and letting the discriminant vanish for a nontrivial solution gives the dispersion relation as:

$$C^2 = \frac{\omega^2}{k^2} = gh\left[\frac{1 - \left(\alpha + \frac{1}{3}\right)(kh)^2}{1 - \alpha(kh)^2}\right] \quad \ldots\ldots (30)$$

where C = phase speed. This relation is similar to Witting's (1984) second-order dispersion relation, which was also used by Murray (1989) and Madsen et al. (1991). However, the new form of the Boussinesq equations presented in this paper is quite different from that of Murray (1989) and Madsen et al. (1991). The previous authors start off with a desired linear dispersion relation and simply add an extra term to the momentum equation to produce the desired characteristics. The depth-averaged velocity is still used as the velocity variable and their equations are applicable in water of constant depth only. The current form of the equations are derived from the classical Euler equations without assuming any dispersion relation a priori. The velocity at an arbitrary distance from the still-water level is used as the velocity variable and the equations are applicable in water of varying depth. The current equations are similar in form to Witting's (1984) second-order

equations. However, Witting's equations are also restricted to water of constant depth.

As noted by Madsen et al. (1991), depending on the velocity variable used or the value of α, different dispersion relations are obtained. If the velocity at the seabed ($z_\alpha = -h$) is used, $\alpha = -1/2$. Alternatively, if the velocity at the still-water level ($z_\alpha = 0$) is used, $\alpha = 0$. The standard form of the Boussinesq equations which uses the depth-averaged velocity corresponds to $\alpha = -1/3$. The exact linear dispersion relation for Airy waves is given by

$$C^2 = gh \frac{\tanh kh}{kh} \quad (31)$$

The phase speeds for different values of α, normalized with respect to the linear-theory phase speed [(31)], are plotted as a function of relative depth in Fig. 1. The relative depth is defined as the ratio of the water depth, h, to the equivalent deep-water wavelength $l_0 = 2\pi g/\omega^2$. The "deep-water" depth limit corresponds to $h/l_0 = 0.5$. The different dispersion equations are all equivalent in relatively shallow water ($h/l_0 < 0.02$), but gradually depart from the exact solution with increasing depth. The velocity at the still-water level gives the poorest fit. The value $\alpha = -2/5$ was obtained by Witting (1984), using a (1,1) Padé approximant of tanh kh. The coefficients of the (1,1) Padé approximation are obtained from the Taylor-series expansion of tanh kh up to $O(\mu^4)$, i.e.

$$\frac{\tanh kh}{kh} = 1 - \frac{1}{3}(kh)^2 + \frac{2}{15}(kh)^4 + O(\mu^6) = \frac{1 + \frac{1}{15}(kh)^2}{1 + \frac{2}{5}(kh)^2} + O(\mu^6) \quad (32)$$

The linear dispersion relation for the standard form of the Boussinesq equations is only accurate up to $O(\mu^2)$:

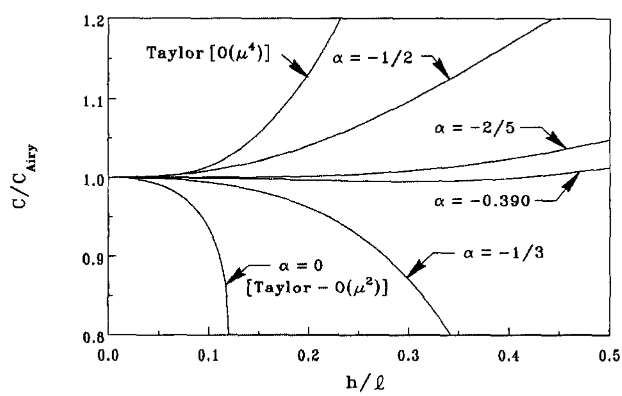

FIG. 1. Comparison of Normalized Phase Speeds for Different Values of α

$$\frac{\tanh kh}{kh} = 1 - \frac{1}{3}(kh)^2 + O(\mu^4) = \frac{1}{1 + \frac{1}{3}(kh)^2} + O(\mu^4) \quad \ldots\ldots\ldots (33)$$

Thus, by varying the value of α, one can change the order of magnitude of the error term in the dispersion relation considerably. Even though both the continuity and momentum equations are only accurate up to the leading order in frequency dispersion, $O(\mu^2)$, the dispersion relation for the coupled set of equations can be accurate up to $O(\mu^4)$. An optimum value of α for the range, $0 < h/l_0 < 0.5$, was obtained by minimizing the sum of the relative error of the phase speed over the entire range. This gave a value, $\alpha = -0.390$, corresponding to the velocity at an elevation $z_\alpha = -0.53h$. The normalized phase speed for the new value of α is also shown in Fig. 1. It gives a maximum difference of less than 2% for the entire range. By comparison, the standard form of the Boussinesq equations ($\alpha = -1/3$) has a phase speed error of 85% at a maximum h/l_0 of 0.48. The new value of α also provides a better match of the phase speed than the Taylor-series expansion of tanh kh up to $O(\mu^4)$.

The group velocity, C_g, which is associated with the propagation of wave energy (or the wave envelope), is also important in wave propagation studies. The wave front, as well as the alternate groups of large and small waves that occur in irregular wave trains, travel at the group velocity. The group velocity for the new form of Boussinesq equations is given by

$$C_g = \frac{d\omega}{dk} = C\left\{1 - \frac{\frac{(kh)^2}{3}}{[1 - \alpha(kh)^2]\left[1 - \left(\alpha + \frac{1}{3}\right)(kh)^2\right]}\right\} \quad \ldots\ldots\ldots (34)$$

The normalized group velocities for different values of α are plotted as a function of relative depth (h/l_0) in Fig. 2. The group velocities are observed to deviate more rapidly from the exact relation than the phase velocities. The new value of α has a maximum error of 12% for the group velocity, while the standard form of the Boussinesq equations ($\alpha = -1/3$) has an error of 100% at a maximum h/l_0 of 0.48.

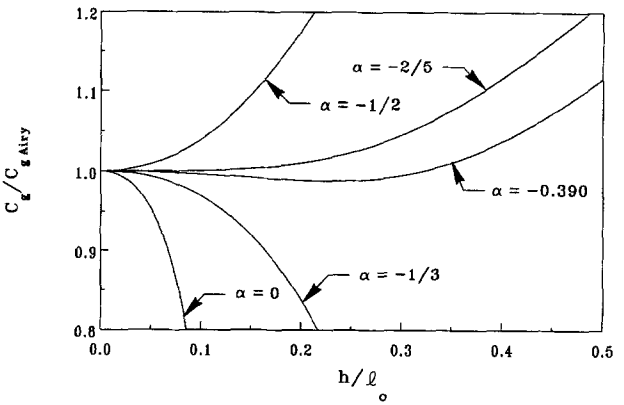

FIG. 2. Comparison of Normalized Group Velocities for Different Values of α

In intermediate water depths with $h/l_0 < 0.3$, the differences between the phase and group velocities of the new Boussinesq model and Airy theory become negligible. An α value of -0.393 gives errors of less than 0.2% for the phase speed and 1% for the group velocity over the entire range. In order to further illustrate the improvement of the dispersion properties of the new set of equations over the standard set of equations, if we apply a 1% maximum error criterion to the phase speed, $\alpha = -1/3$ gives a maximum h/l_0 of 0.12 while $\alpha = -0.393$ gives a maximum h/l_0 of 0.42. Applying the same error criterion to the group velocity gives $h/l_0 = 0.06$ for $\alpha = -1/3$ and $h/l_0 = 0.30$ for $\alpha = -0.393$. The new set of Boussinesq equations are thus applicable to water depths three to five times deeper than could be previously modeled with the same level of accuracy in the linear dispersion characteristics.

Nonlinear Properties

In an irregular sea state, the different frequency components interact to generate forced waves at the sum and difference frequencies of the primary waves because of the nonlinear boundary conditions at the free surface. The Boussinesq equations are weakly nonlinear and, thus, are able to simulate the generation of the higher-order forced waves. For the Laplace equation, Longuet-Higgins and Stewart (1962) derived expressions for the magnitude of the low-frequency component of the second-order forced waves. Dean and Sharma (1981) derived similar expressions for both the lower and higher harmonics in multidirectional wave fields. In this section, we shall derive expressions for the magnitude of the second-order forced waves in water of constant depth from the new Boussinesq equations. Consider a wave train consisting of two small amplitude periodic waves with frequencies ω_1 and ω_2, and amplitudes a_1 and a_2. The water-surface elevation is given by

$$\eta^{(1)}(x, t) = a_1 \cos(k_1 x - \omega_1 t) + a_2 \cos(k_2 x - \omega_2 t) \quad \ldots\ldots\ldots\ldots\ldots (35)$$

where k_1 and k_2 = the respective wave numbers. The individual waves satisfy the first-order or linearized form of the Boussinesq equations [(27) and (28)]. Therefore, the horizontal velocity can be written as:

$$u_\alpha^{(1)}(x, t) = \frac{\omega_1}{k_1' h} a_1 \cos(k_1 x - \omega_1 t) + \frac{\omega_2}{k_2' h} a_2 \cos(k_2 x - \omega_2 t) \quad \ldots\ldots\ldots (36)$$

where $k_1' = k_1\{1 - [\alpha + (1/3)](k_1 h)^2\}$; and $k_2' = k_2\{1 - [\alpha + (1/3)](k_2 h)^2\}$. The equations for the forced waves that satisfy the Boussinesq equations at second order in wave amplitude can be written as:

$$\eta_t^{(2)} + h u_{\alpha x}^{(2)} + \left(\alpha + \frac{1}{3}\right) h^3 u_{\alpha xxx}^{(2)} = -\eta^{(1)} u_{\alpha x}^{(1)} - u_\alpha^{(1)} \eta_x^{(1)} \quad \ldots\ldots\ldots (37)$$

$$u_{\alpha t}^{(2)} + g\eta_x^{(2)} + \alpha h^2 u_{\alpha xxt}^{(2)} = -u_\alpha^{(1)} u_{\alpha x}^{(1)} \quad \ldots\ldots\ldots\ldots\ldots\ldots\ldots\ldots (38)$$

The second-order wave will consist of a subharmonic at the difference frequency $\omega_- = \omega_1 - \omega_2$, and higher harmonics at the sum frequencies $2\omega_1$, $2\omega_2$, and $\omega_+ = \omega_1 + \omega_2$. It can be expressed as:

$$\eta^{(2)}(x, t) = a_1 a_2 G_\pm(\omega_1, \omega_2)\cos(k_\pm x - \omega_\pm t) + \frac{a_1^2}{2} G_+(\omega_1, \omega_1)\cos(2k_1 x$$

$$- 2\omega_1 t) + \frac{a_2^2}{2} G_+(\omega_2, \omega_2)\cos(2k_2 x - 2\omega_2 t) \quad \ldots\ldots\ldots\ldots\ldots\ldots (39)$$

where $k_\pm = k_1 \pm k_2$; and $G_\pm(\omega_1, \omega_2)$ = a quadratic transfer function that relates the amplitude of the second-order wave to the first-order amplitudes. The difference frequency component, which is commonly referred to as the set-down component, is important in many coastal engineering problems such as the motions of moored ships in harbors and sediment transport on beaches. It travels at the velocity of the wave group, ω_-/k_-. The sum frequency waves travel at the phase velocities of the individual waves and distort the wave profile, making the crest elevations larger than the trough elevations.

By substituting (35) and (36) into (37) and (38), and solving for the amplitudes of the second-order surface elevation and velocity, we obtain an expression for the quadratic transfer function:

$$G_\pm(\omega_1, \omega_2) = \frac{\omega_\pm k_\pm h[1 - \alpha(k_\pm h)^2][\omega_1 k_2' h + \omega_2 k_1' h] + \omega_1\omega_2(k_\pm h)^2\left[1 - \left(\alpha + \frac{1}{3}\right)(k_\pm h)^2\right]}{\left\{\omega_\pm^2[1 - \alpha(k_\pm h)^2] - gk_\pm^2 h\left[1 - \left(\alpha + \frac{1}{3}\right)(k_\pm h)^2\right]\right\} 2k_1' k_2' h^3} \quad \ldots\ldots\ldots\ldots (40)$$

The quadratic transfer function of the Boussinesq equations is compared to that of the second-order Laplace equation in Fig. 3 for an example where the period of the wave group is ten times the average of the individual wave periods, i.e., $\omega_2 - \omega_1 = 0.1\omega$, where $\omega = (\omega_1 + \omega_2)/2$. The transfer function is plotted against h/l_0, where $l_0 = 2\pi g/\omega^2$. The Boussinesq model underestimates the magnitude of the set-down wave and second harmonic at the deep-water depth limit by 65% and 45%, respectively. Therefore, it cannot accurately simulate nonlinear effects in deep water. To be able to reasonably simulate nonlinear effects, the Boussinesq model should be restricted to the range $0 < h/l_0 < 0.3$.

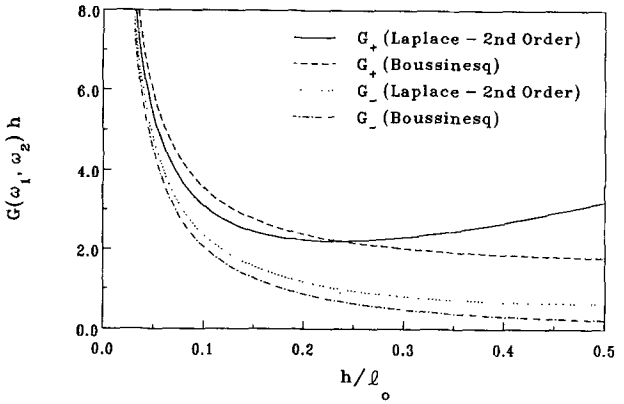

FIG. 3. Comparison of Quadratic Transfer Function of Boussinesq and Second-Order Laplace Theories ($\omega_2/\omega_1 = 1.1$)

NUMERICAL SOLUTION

Finite Difference Scheme

The one-dimensional version of the governing differential equations [(25*a*) and (25*b*)] have been solved numerically using a finite difference method. An iterative Crank-Nicolson method is employed, with a predictor-corrector scheme used to provide the initial estimate. The method consists essentially of three stages. At any given time step $t = j\Delta t$, we predict the values of the variables at $t = [j + (1/2)]\Delta t$ using the known values at $t = j\Delta t$. The estimated values at $t = [j + (1/2)]\Delta t$ are then used in the corrector stage to compute the values at $t = (j + 1)\Delta t$. Finally, the computed values at $t = (j + 1)\Delta t$ are used as an initial guess in an iterative scheme, which is repeated until convergence.

The partial derivatives are approximated using a forward difference scheme for the time variable and a central difference scheme for the space variable. The following finite difference operators can be defined:

$$\delta_x u_{i,j} = \frac{u_{i+1,j} - u_{i-1,j}}{2\Delta x} \quad \ldots\ldots (41a)$$

$$\delta_x^2 u_{i,j} = \frac{u_{i+1,j} - 2u_{i,j} + u_{i-1,j}}{\Delta x^2} \quad \ldots\ldots (41b)$$

$$\delta_x^3 u_{i,j} = \frac{u_{i+2,j} - 2u_{i+1,j} + 2u_{i-1,j} - u_{i-2,j}}{2\Delta x^3} \quad \ldots\ldots (41c)$$

where $u_{i,j}$ = the value of a variable $u(u_\alpha$ or $\eta)$ at $x = i\Delta x$; $t = j\Delta t$; and Δx and Δt = the spatial-grid size and time-step size, respectively. The finite difference approximations of the partial derivatives at different stages of the numerical procedure are listed in Table 1. The finite difference scheme is third-order accurate with truncation errors of $O(\Delta x^3, \Delta t^3)$. The approximation of the first-order time and spatial derivatives include terms of $O(\Delta x^2, \Delta t^2)$, which involve third-order derivatives. These terms can be important to the dispersion characteristics of the numerical model, since the dispersion terms in the governing equations involve similar derivatives. The terms with higher-order time derivatives were evaluated using information from the two previous time steps:

$$u_{ttt} = \frac{u_{j+1} - 3u_j + 3u_{j-1} - u_{j-2}}{\Delta t^3} \quad \ldots\ldots (42)$$

TABLE 1. Finite Difference Approximations

Variable (1)	Predictor stage (2)	Corrector stage (3)	Iterative stage (4)
u	$u_{i,j}$	$u_{i,j+(1/2)}$	$(1/2)(u_{i,j} + u_{i,j+1})$
u_t	$[u_{i,j+(1/2)} - u_{i,j}]/(\Delta t/2)$	$(u_{i,j+1} - u_{i,j})/\Delta t$	$(u_{i,j+1} - u_{i,j})/\Delta t - u_{ttt}(\Delta t^2/24)$
u_x	$\delta_x u_{i,j}$	$\delta_x u_{i,j+(1/2)}$	$(1/2)\delta_x(u_{i,j} + u_{i,j+1}) - u_{xxx}(\Delta x^2/6) - u_{xtt}(\Delta t^2/8)$
u_{xt}	$\delta_x[u_{i,j+(1/2)} - u_{i,j}]/(\Delta t/2)$	$\delta_x(u_{i,j+1} - u_{i,j})/\Delta t$	$\delta_x(u_{i,j+1} - u_{i,j})/\Delta t$
u_{xx}	$\delta_x^2 u_{i,j}$	$\delta_x^2 u_{i,j+(1/2)}$	$(1/2)\delta_x^2(u_{i,j} + u_{i,j+1})$
u_{xxt}	$\delta_x^2[u_{i,j+(1/2)} - u_{i,j}]/(\Delta t/2)$	$\delta_x^2(u_{i,j+1} - u_{i,j})/\Delta t$	$\delta_x^2(u_{i,j+1} - u_{i,j})/\Delta t$
u_{xxx}	$\delta_x^3 u_{i,j}$	$\delta_x^3 u_{i,j+(1/2)}$	$(1/2)\delta_x^3(u_{i,j} + u_{i,j+1})$

$$u_{xtt} = \frac{3u_{x,j+1} - 7u_{x,j} + 5u_{x,j-1} - u_{x,j-2}}{2\Delta t^2} \quad \ldots\ldots (43)$$

The numerical solution procedure involves solving an explicit expression for η and a tridiagonal matrix for u_α in the predictor and corrector stages, and tridiagonal matrices for both variables in the iterative stage. Tridiagonal matrices contain only diagonal and adjacent off-diagonal terms and can be solved efficiently using a Gaussian elimination process. In all the examples considered in this paper, a maximum of two iterations per time step was required to achieve convergence.

Stability Considerations

Although the Crank-Nicolson method is unconditionally stable for a single linear equation, the stability of the scheme for a set of coupled equations is not guaranteed. A stability analysis was therefore carried out for the finite difference solution of the linearized form of the constant depth equations. The scheme can be written in the matrix form as:

$$\mathbf{A}\mathbf{U}_{j+1} = \mathbf{B}\mathbf{U}_j \quad \ldots\ldots (44)$$

where $\mathbf{U} = (\eta, u_\alpha)^T$. If we assume a periodic wave of the form given by (29) with $x = i\Delta x$ and $t = j\Delta t$, the components of the matrices can be written as:

$$A_{11} = B_{11} = 1 \quad \ldots\ldots (45a)$$

$$A_{12} = -B_{12} = \frac{h\Delta t}{2\Delta x} \sin k\Delta x \left[1 - 2\left(\alpha + \frac{1}{3}\right)\frac{h^2}{\Delta x^2}(1 - \cos k\Delta x)\right] \quad (45b)$$

$$A_{21} = -B_{21} = \frac{g\Delta t}{2\Delta x} \sin k\Delta x \quad \ldots\ldots (45c)$$

$$A_{22} = B_{22} = 1 - 2\alpha\frac{h^2}{\Delta x^2}(1 - \cos k\Delta x) \quad \ldots\ldots (45d)$$

The amplification matrix of the method is $\mathbf{G} = \mathbf{A}^{-1}\mathbf{B}$, and for the computational procedure to the stable, the eigenvalues of the amplification matrix have to be less than unity. This gives the following stability condition:

$$\frac{gh\Delta t^2}{4\Delta x^2} \sin^2 k\Delta x < \frac{1 - 2\alpha\dfrac{h^2}{\Delta x^2}(1 - \cos k\Delta x)}{1 - 2\left(\alpha + \dfrac{1}{3}\right)\dfrac{h^2}{\Delta x^2}(1 - \cos k\Delta x)} \quad \ldots\ldots (46)$$

If the dispersion terms are neglected, the corresponding condition for long waves can be expressed in terms of the Courant number, C_R as

$$C_R = \sqrt{gh}\frac{\Delta t}{\Delta x} < 2 \quad \ldots\ldots (47)$$

Boundary Conditions

To solve the governing equations, appropriate physical conditions have to be imposed at the boundaries of the computational domain. In the examples considered in this paper, this requires specification of the waves

propagating into the domain, and absorption of the waves propagating out. Let the computational domain be defined by $0 < x < x_r$, with a uniform grid size Δx such that $x_i = i\Delta x$, $i = 0, 1, \ldots, N$. The interior points are denoted by $i = 1, 2, \ldots, N-1$, while the boundary points are represented by $i = 0$ and $i = N$. At the incident wave boundary ($x = 0$), the time series of the water-surface elevation $\eta(0, t)$, velocity $u_\alpha(0, t)$, and second spatial derivative of the velocity $u_{\alpha xx}(0, t)$ are specified.

For small amplitude regular waves, the velocity can be obtained from the surface elevation using the continuity equation shown in (27), and is given by

$$u_\alpha(0, t) = \frac{\omega}{kh_0\left[1 - \left(\alpha + \frac{1}{3}\right)(kh_0)^2\right]}\eta(0, t) \quad \ldots\ldots\ldots\ldots\ldots\ldots (48)$$

Irregular wave conditions can be obtained from a linear superposition of regular waves. If the wave field at the incident boundary is significantly nonlinear, the incident water surface elevation and velocity would have to be modified to include the bound subharmonics and super-harmonics. If the forced waves are neglected, the model would generate free second-order waves with the same magnitude as the forced waves but 180° out of phase at the incident boundary to satisfy the linear condition. However, the examples presented in this paper consider only small amplitude waves at the incident boundary.

In the finite difference computations, the third-order spatial derivatives at the first and last interior points are evaluated using

$$u_{xxx}|_{1,j} = \frac{u_{3,j} - 2u_{2,j} + u_{1,j} - \Delta x^2 u_{xx}|_{0,j}}{2\Delta x^3} \quad \ldots\ldots\ldots\ldots\ldots\ldots (49)$$

$$u_{xxx}|_{N-1,j} = \frac{u_{N,j} - 3u_{N-1,j} + 3u_{N-2,j} - u_{N-3,j}}{\Delta x^3} \quad \ldots\ldots\ldots\ldots\ldots\ldots (50)$$

At the outgoing wave boundary, a nonreflecting condition is used to absorb the waves. Consider a regular wave train consisting of an incident wave of unit amplitude and a reflected wave with amplitude r and associated phase shift ϕ. This can be expressed as:

$$\eta(x, t) = \exp[i(kx - \omega t)] + r\exp[-i(kx + \omega t + \phi)] \quad \ldots\ldots\ldots\ldots (51)$$

For the reflected wave amplitude to be identically zero, it can easily be shown that the following condition has to be satisfied:

$$\eta_t + C\eta_x = 0 \quad \ldots\ldots\ldots\ldots\ldots\ldots\ldots\ldots\ldots\ldots\ldots\ldots\ldots\ldots\ldots\ldots (52)$$

where $C = \omega/k$. The foregoing equation is equivalent to the Sommerfeld (1949) radiation condition used in potential flow theory. For irregular waves, an approximate phase velocity at the absorbing boundary can be calculated using the average zero-crossing period of the input wave train.

In the numerical implementation, the first-order derivative at the absorbing boundary is approximated using a one-sided, second-order accurate difference scheme:

$$\eta_x|_{N,j} = \frac{3\eta_{N,j} - 4\eta_{N-1,j} + \eta_{N-2,j}}{2\Delta x} \quad \ldots\ldots\ldots\ldots\ldots\ldots\ldots (53)$$

Although (52) is a perfectly absorbing condition, there will be a small amount of reflection from the boundary due to truncation errors, the initial transient, steep waves, and the approximation of the phase velocity for irregular waves. The use of (48) to relate u_α to η also introduces some free second-order waves that propagate back to the incident boundary.

If partial wave reflection is desired from the boundary, a more general form of the boundary condition in (52) that includes the effect of partial reflection is given by

$$\frac{1 - r\cos\phi}{1 + r\cos\phi}\eta_t + C\eta_x = 0 \quad \ldots\ldots\ldots\ldots\ldots\ldots\ldots\ldots\ldots\ldots\ldots\ldots (54)$$

In cases where there is significant wave reflection, the boundary condition at the incident-wave boundary has to be modified to absorb the reflected waves. The new incident-wave boundary condition can be written as

$$\eta_t - C\eta_x - 2\eta_{0t} = 0 \quad \ldots\ldots\ldots\ldots\ldots\ldots\ldots\ldots\ldots\ldots\ldots\ldots (55)$$

where η_{0t} = the time derivative of the incident water-surface elevation η_0.

DESCRIPTION OF EXPERIMENTS

Laboratory experiments have been performed to evaluate the ability of the new Boussinesq model to simulate the nonlinear shoaling of regular and irregular waves on a constant slope beach. The tests were conducted in the multidirectional wave basin of the Hydraulics Laboratory, National Research Council of Canada, Ottawa. The basin is 30 m wide, 20 m long and 3 m deep. It is equipped with a 60-segment wave generator capable of producing regular and irregular, unidirectional and multidirectional waves. A 1:25 constant slope beach with an impermeable concrete cover was constructed in the basin. The toe of the beach was located 4.6 m from the waveboard. A water depth of 0.56 m in the constant depth portion of the basin was used for all the tests. The water-surface elevation along the centerline of the basin was measured with a linear array of 23 capacitance-wire wave probes. The spacing between the wave probes varied from 0.3 m to 1.6 m. The experimental layout is shown in Fig. 4.

The test conditions consisted of solitary waves, normal and oblique regular and irregular waves, and irregular multidirectional sea states. However, the discussion in this paper is limited to normally incident regular and irregular waves. The regular waves had periods T ranging from 0.85 s to 3.5 s and heights H ranging from 0.04 m to 0.10 m. An irregular wave time series was synthesized from a Joint North Sea Wave Project (JONSWAP) spectrum using the random phase method (e.g., Funke and Mansard 1984). The sea state, with a recycling period of 819.2 s, was simulated at a time interval of 0.05 s. The simulated sea state had a peak frequency f_p of 0.67 Hz,

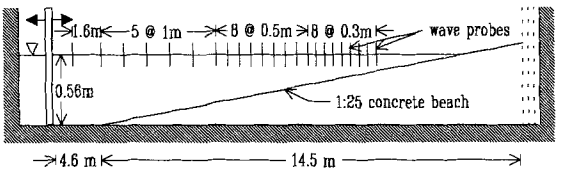

FIG. 4. Experimental Setup

significant wave height $H_{m0} = 0.09$ m, and $\gamma = 3.3$. Linear theory was used to relate the wave-board displacement to the water-surface elevation with no attempt made to correct for the generation of free second-order waves. The data acquisition system was synchronized to start as soon as the wave generator was started, and the data were sampled at a frequency of 20 Hz.

NUMERICAL AND EXPERIMENTAL RESULTS

Regular Waves

The standard form of the Boussinesq equations cannot simulate the propagation of deep-water waves since its dispersion relation does not converge for $h/l_0 > 0.48$. A numerical experiment was thus performed to evaluate the ability of the new Boussinesq model to simulate the propagation of regular waves in deep water. Consider a wave train with period $T = 0.85$ s and height $H = 0.05$ m, propagating in a channel with a uniform depth of

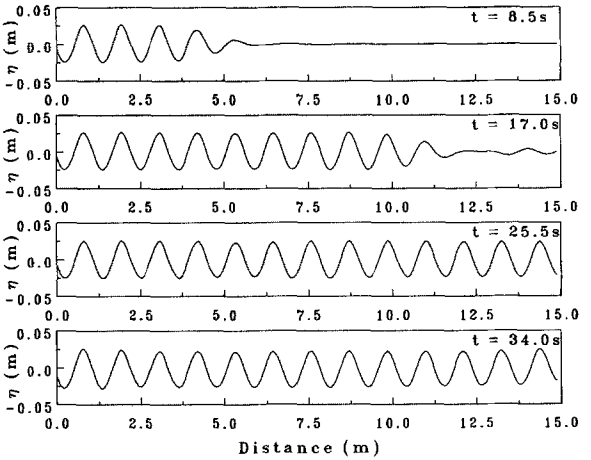

FIG. 5. Numerical Simulation of Propagation of Regular Wave in Water of Constant Depth ($T = 0.85$ s, $h = 0.56$ m)

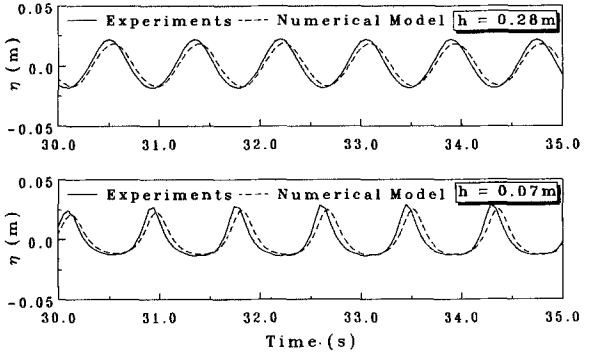

FIG. 6. Comparison of Time Series of Regular Wave Shoaling on Constant Slope Beach ($T = 0.85$ s)

0.56 m. The relative depth, h/l_0, is 0.50. The absorbing boundary is located 15 m from the incident boundary. The computations were carried out using $\Delta x = l_0/32$ and $\Delta t = T/32$. Fig. 5 shows the spatial profile of the propagating wave at different instants of time. The maximum variation of wave height in the channel before any reflection from the absorbing boundary is less than 0.5%. The new equations are able to model the propagation of effectively deep-water waves in water of constant depth.

The results of the new Boussinesq model have also been compared with data obtained from the laboratory experiments. The first example is an incident deep-water wave ($T = 0.85$ s, $H_0 = 0.04$ m, and $h_0/l_0 = 0.5$), propagating on a beach with an average slope of 1:25. The water depth at the offshore boundary is 0.56 m, while the depth at the absorbing boundary is 0.07 m. The measured water-surface elevation time history at the toe of the slope was resampled to a new Δt of 0.025 s and input to the numerical model as the offshore boundary condition. The computations were performed with a grid size $\Delta x = l_0/32$. Fig. 6 shows a comparison of the measured surface elevation with results obtained from the numerical model at depths of 0.07 m and 0.28 m. The numerical results lag slightly behind the laboratory results because of differences in the phase and group velocities. The numerical model also underestimates the wave height at the intermediate and shallow depths by about 10%.

The next example investigated was the shoaling of an intermediate-depth wave ($T = 1.0$ s, $H_0 = 0.066$ m, $h_0/l_0 = 0.36$). The numerical simulations were performed with grid resolutions $\Delta x = l_0/40$, and $\Delta t = T/40$. The absorbing boundary was located at a water depth of 0.10 m, which is approximately where the waves were observed to start breaking in the laboratory. The time series of the measured surface elevation at water depths of 0.24 m and 0.10 m are compared with predictions from the new Boussinesq model ($\alpha = -0.392$) and the standard Boussinesq model ($\alpha = -1/3$) in Fig. 7. The differences between the phase and group velocities of the standard Boussinesq model and Airy theory are 25% and 70%, respectively, at the incident boundary. This leads to the observed phase lag and wave height differences between the measured data and the standard Boussinesq model.

In contrast, the new Boussinesq model predicts the observed wave heights at both the intermediate and shallow depths reasonably well. There are, however, slight differences in the water-surface profile at the shallow depth. The Boussinesq wave profile is not as asymmetric about the vertical plane as the measured profile. This is partly due to the fact that the Boussinesq model is only a weakly nonlinear model, and the amplitudes and phase shifts of the higher harmonics may not be accurately simulated. It was also observed in the experiments that run-down currents generated after wave breaking tend to steepen the waves further.

A much better match of the asymmetric wave profile was obtained for incident waves in shallower water. Fig. 8 shows a comparison of the time series of the surface elevation for a wave of $T = 1.5$ s ($h_0/l_0 = 0.16$) at water depths of 0.24 m and 0.14 m. The agreement between the experimental data and numerical model is surprisingly good, especially since the laboratory waves were breaking on the slope and generating currents which distorted the wave field. The results show that the Boussinesq model is able to simulate the transformation of linear waves in intermediate water to very steep, near breaking waves in shallow water. The effect of bottom friction was not included in the numerical model. The comparisons of the numerical and experimental results seem to indicate that bottom friction was not an

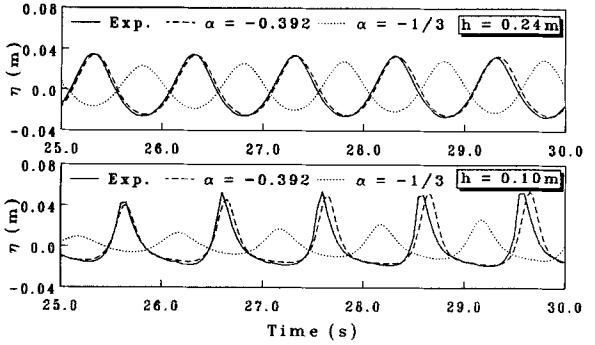

FIG. 7. Comparison of Time Series of Regular Wave Shoaling on Constant Slope Beach (T = 1.0 s)

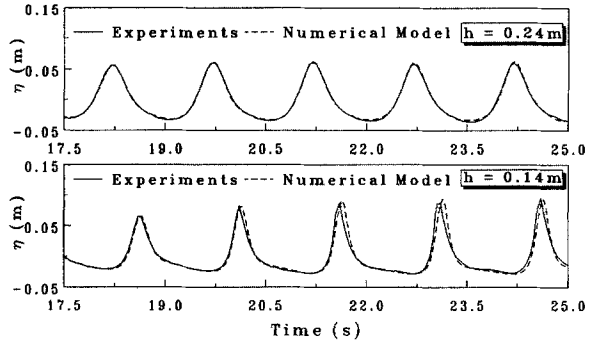

FIG. 8. Comparison of Time Series of Regular Wave Shoaling on Constant Slope Beach (T = 1.5 s)

important factor for the concrete beach, wave conditions, and beach slope used in these experiments.

Irregular Waves

A more important application of the new Boussinesq model is to the shoaling of irregular waves, where existing models are either linear for arbitrary water depths or nonlinear for relatively shallow water depths. The new Boussinesq model is now used to examine the shoaling of irregular waves from "deep" to shallow water. Consider the sea state synthesized from a JONSWAP spectrum with H_{m0} = 0.09 m, f_p = 0.67 Hz, and γ = 3.3. The relative depth at the incident boundary is 1.0 for the maximum frequency of interest ($2.5f_p$). The time series of the surface elevation measured at the toe of the slope was input to the numerical model as the offshore boundary condition. The time series had a duration of 819.2 s and time interval of 0.05 s. The finite difference computations were performed with a grid size Δx = 0.04 m and α = −0.390. The absorbing boundary was located at a water depth of 0.20 m, just ahead of the wave breaking zone.

Fig. 9 shows a comparison of the measured and numerically predicted water-surface elevations at the shallow depth of 0.20 m. In the earlier portion of the time record (10–30 s), the measured surface elevation is well predicted

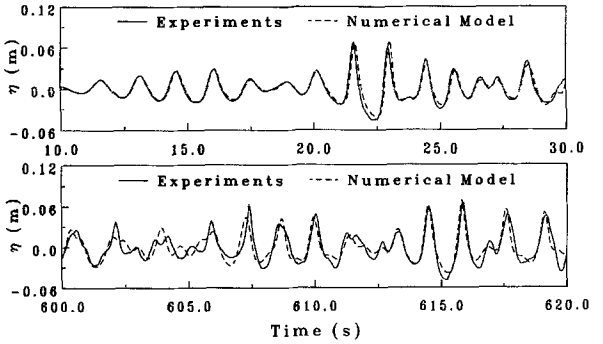

FIG. 9. Comparison of Measured and Predicted Water-Surface Elevations for Irregular Wave Train (h = 0.20 m)

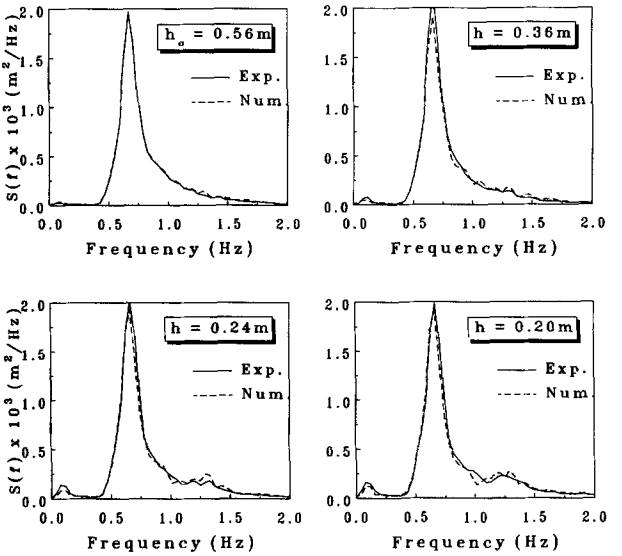

FIG. 10. Spectral Densities of Surface Elevation of Irregular Wave Train Propagating on Constant Slope Beach

by the numerical model. After a few waves have propagated through the absorbing boundary, differences between the numerical and experimental results become more noticeable. This is partly because the linear condition [(52)] applied at the absorbing boundary is only an approximation of the complex physical process occurring at that boundary. The comparison for the 600–620s portion of the time record shows that the numerical model is still able to reproduce the important characteristics of the laboratory data despite its limitations.

The spectral densities of the measured and predicted water-surface elevation time histories at different water depths are compared in Fig. 10. The spectral estimates were averaged over frequency bands of width 0.04 Hz (130 degrees of freedom). As the wave train shoals, there is an increase

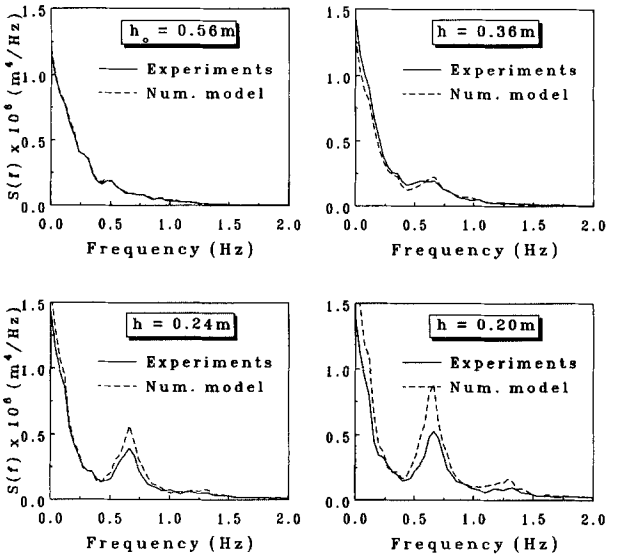

FIG. 11. Spectral Densities of Square of Envelope of Surface Elevation of Irregular Wave Train Propagating on Constant Slope Beach

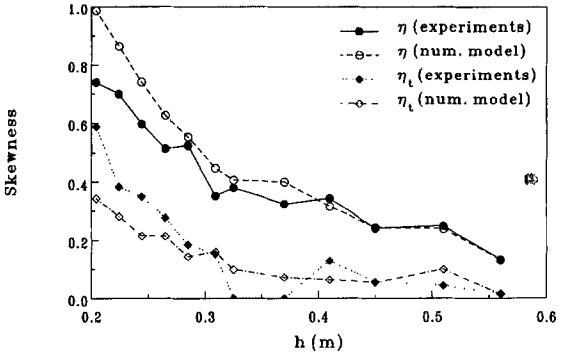

FIG. 12. Skewness Variation with Water Depth

in the low- and high-frequency wave energy due to the amplification of the bound harmonics and the cross-spectral transfer of energy. The new Boussinesq model is seen to reasonably predict the observed growth of the sub- and superharmonics. The long-period wave activity in shallow water consists of incident forced waves accompanying the wave groups plus the free long waves that are reflected back to the offshore after the waves break and run up the slope. Although the numerical model generates some free long waves at the absorbing boundary because of the linear nature of the boundary condition, the long waves are not accurately reproduced in the model since it does not include wave breaking and runup.

The characteristics of wave groups in irregular wave trains also substantially change during the shoaling process. The properties of wave groups in shallow water are important in certain coastal engineering problems

such as the stability of rubble-mound breakwaters, slow drift oscillations of moored vessels, and the erosion of beaches. One indicator of wave grouping is the envelope of the wave train. The wave envelope can be calculated from the Hilbert transform of the time series of the surface elevation without applying any filters. Fig. 11 shows the spectral densities of the square of the surface-elevation envelope at different water depths. As the wave shoals, the variance of the square of the wave envelope increases. A secondary peak also appears around the peak frequency, f_p, of the incident wave spectrum. This peak is due to the nonlinear combination of waves with frequencies around f_p and $2f_p$, which produces components around f_p. The Boussinesq model reproduces the observed trends in the evolution of the envelope spectra.

Nonlinear effects in shallow water also affect the probability distributions of the surface elevation and its time derivative. The crest elevations are larger than the trough elevations, leading to a skewed, non-Gaussian probability distribution of the surface elevation, or horizontal asymmetry. The steepening of the crest front leads to a skewed distribution of the time derivative of the surface elevation or vertical asymmetry. The horizontal and vertical asymmetry are also related to the real and imaginary parts of the surface-elevation bispectrum, respectively. Fig. 12 shows a plot of the skewness of the water-surface elevation and its time derivative as a function of water depth. The skewness of both η and η_t increase as the depth decreases with the horizontal asymmetry more affected by shoaling than the vertical asymmetry. The Boussinesq model overestimates the skewness values for η because it does not include wave breaking. It predicts larger crest elevations for some of the breaking waves. The underestimation of the skewness values for η_t is because the Boussinesq wave profiles are not as steep as the observed profiles just prior to breaking.

CONCLUSIONS

A new set of Boussinesq-type equations has been derived, using the velocity at an arbitrary distance from the still-water level as the velocity variable instead of the commonly used depth-averaged velocity. In intermediate and deep water, the linear dispersion characteristics of the new equations are strongly dependent on the choice of the velocity variable. Selecting a velocity close to middepth as the velocity variable significantly improves the dispersion properties of the new Boussinesq model, making it applicable to a wider range of water depths. A finite difference method has been used to solve the equations for one horizontal dimension. The results of the numerical procedure have been compared to laboratory data. Good agreement was obtained for the shoaling of regular waves from intermediate to shallow water and irregular waves from deep to shallow water. The numerical model was able to reproduce several nonlinear effects that occur during shoaling such as the generation of longer- and shorter-period waves, an increase in horizontal and vertical asymmetries and the evolution of wave groups. The new Boussinesq model does not violate any of the assumptions of Boussinesq theory but simply extends the range of applicability of the equations. It represents a practical tool for simulating the nonlinear transformation of nonbreaking, irregular, multidirectional waves in water of varying depth.

ACKNOWLEDGMENTS

Part of this work was completed while the writer was visiting the Port and Harbour Research Institute, Yokosuka, Japan. The writer would like to thank the Japan International Science and Technology Exchange Center for the fellowship that enabled him to visit Japan. The writer also wishes to thank T. Takayama and E. P. D. Mansard for many stimulating discussions. The assistance of H. Claes and B. Gow in the experimental work is gratefully acknowledged.

APPENDIX I. REFERENCES

Dean, R. G., and Sharma, J. N. (1981). "Simulation of wave systems due to nonlinear directional spectra." *Proc. Int. Symp. on Hydrodyn. in Oc. Engrg.*, Norwegian Hydrodynamics Laboratory, Trondheim, Norway, 1211–1222.

Freilich, N. H., and Guza, R. T. (1984). "Nonlinear effects on shoaling surface gravity waves." *Phil Trans.*, Royal Society of London, A311, 1–41.

Funke, E. R., and Mansard, E. P. D. (1984). "The NRCC random wave generation package." *Inst. for Mech. Engrg. Tech. Report TR-HY-002*, Nat. Res. Council, Ottawa, Ontario.

Longuet-Higgins, M. S., and Stewart, R. W. (1962). "Radiation stress and mass transport in gravity waves, with application to 'surf beats.'" *J. Fluid Mech.*, 13, 481–504.

Madsen, P. A., Murray, R., and Sorensen, O. R. (1991). "A new form of the Boussinesq equations with improved linear dispersion characteristics." *Coast. Engrg.*, 15, 371–388.

McCowan, A. D. (1987). "The range of application of Boussinesq type numerical short wave models." *Proc., 22nd Congress, International Association for Hydraulic Research*, Lausanne, Switzerland, 379–384.

McCowan, A. D., and Blackman, D. R. (1989). "The extension of Boussinesq type equations to modelling short waves in deep water." *Proc., 9th Australasian Conf. on Coast. and Oc. Engrg.*, Institution of Engineers, Adelaide, Australia, 412–416.

Mei, C. C. (1983). *The applied dynamics of ocean surface waves*. John Wiley, New York, N.Y.

Murray, R. J. (1989). "Short wave modelling using new equations of Boussinesq type." *Proc., 9th Australasian Conf. on Coast. and Oc. Engrg.*, Institution of Engineers, Adelaide, Australia, 331–336.

Peregrine, D. H. (1967). "Long waves on a beach." *J. Fluid Mech.*, 27, 815–827.

Phillips, O. M. (1977). *Dynamics of the upper ocean*. Cambridge Univ. Press, London, England.

Sommerfeld, A. (1949). *Partial differential equations in physics*. Academic Press, New York, N.Y.

Witting, J. M. (1984). "A unified model for the evolution of nonlinear water waves." *J. Computational Physics*, 56, 203–236.

Yoon, S. B., and Liu, P. L.-F. (1989). "Interactions of currents and weakly nonlinear water waves in shallow water." *J. Fluid Mech.*, 205, 397–419.